A Comparison of the Cell Lines Used In Meningoma Research

Brian T. Ragel, M.D., William T. Couldwell, M.D., Ph.D., David L. Gillespie, Ph.D., Merideth M. Wendland, M.D., Kum Whang, M.D., Ph.D., Randy L. Jensen M.D., Ph.D.

Department of Neurosurgery, University of Utah School of Medicine, Salt Lake City, Utah, 84132 (BTR, WTC, DLG, RLJ); Huntsman Cancer Institute, Salt Lake City, Utah, 84112 (BTR, WTC, DLG, MMW, KW, RLJ); Department of Radiation Oncology, University of Utah School of Medicine, Salt Lake City, Utah, 84132 (MMW)

Department of Neurosurgery, Yonsei University, Wonju, Korea (KW)

Corresponding Author:

Randy Jensen, M.D. Ph.D.

Department of Neurosurgery, University of Utah

30 North 1900 East, Suite 3B409

Salt Lake City, UT 84132

Phone: 801-581-6908

Fax: 801-585-4385

Email: randy.jensen@hci.utah.edu

UU IR Author Manuscript

ABSTRACT

Background: Immortal cell lines and cell lines derived from operative specimens transplanted into animal models are used in meningioma research. We address two criticisms of the mouse xenograft flank tumor model: Why are tumor induction rates derived from operative specimens low and inconsistent? Are flank tumors meningiomas?

Methods: Meningioma cell cultures were processed for Giemsa-band karyotyping and flow cytometry. Mouse flank tumors induced subcutaneously were analyzed microscopically, immunohistochemically, and ultrastructurally. G-band studies identified meningiomas with simple karyotype (≤ 1 chromosomal abnormality) or complex karyotype (multiple chromosomal abnormalities).

Results: Cell cultures with complex karyotypes (IOMM-Lee, CH-157 MN, 2 operative specimens) grew rapidly *in vitro* and induced tumors in 49/50 (98%) animals. Meningioma cell cultures with simple karyotypes grew slowly *in vitro* and showed small, non-growing tumors in mouse flanks (10/10). Meningioma flank tumors were vimentin positive with ultrastructural features consistent with meningiomas. Cell cultures with complex karyotypes grew faster in cell culture and consistently induced flank tumors, unlike meningiomas with simple karyotypes.

Conclusions: Meningioma cell lines transplanted into flanks of nude mice exhibit microscopic, immunohistochemical, and ultrastructural features of meningiomas. The ease of monitoring tumor growth in the subcutaneous mouse flank model is its primary advantage, although we recognize an intracranial location is more biologically desirable.

UU IR Author Manuscript

KEY WORDS: CH-157 MN; IOMM-Lee; Meningioma; Xenograft Mouse Model

RUNNING HEAD: Cell lines involved with meningioma research

UU IR Author Manuscript

INTRODUCTION

Meningiomas are slow-growing, benign tumors that arise from the central nervous system meninges [2]. Specialized meningothelial cells called arachnoid cap cells are the cells of origin of meningiomas. These cells are most common within the arachnoid villi but may be present throughout the craniospinal arachnoid space. Meningiomas account for approximately 20% of all primary adult intracranial tumors. They are more common in women (2:1) and generally occur in older patients. Meningiomas are graded as benign (approximately 91% of meningiomas), atypical (5%), and anaplastic/malignant (4%) [10, 22]. The grading of meningiomas takes into account both the tumor subtypes known to have a higher rate of recurrence and specific histologic features suggesting a more aggressive biology [6, 21]. Although most meningiomas can now be removed safely, their intrinsic biology and location are still the main determinants of the overall outcome of the patient [6, 21, 35].

The study of meningioma biology and possible treatment regimes involves *in vitro* and *in vivo* studies on immortal cell lines, as well as cell lines derived from operative specimens [14, 18, 36, 37]. Cell culture experiments are not necessarily a reflection of *in vivo* responses, so meningioma animal models were developed [25]. Transplantation of human meningiomas into guinea pig eyes was first described in 1945 [11]. Since that time, several xenograft animal transplantation models have been described to include the chorioallantoic membrane of the duck and chick, and the subcutis, subrenal capsule, flank, brain, and skull base of athymic mice [23-26, 30, 38, 40]. Obviously, the intracranial model is the most biologically desirable, but it is limited by the difficulty in obtaining direct serial measurements. The subrenal capsule has high tumor induction

UU IR Author Manuscript

rates, but transplantation to this location is technically challenging and does not allow for direct serial measurements. Flank models were initially limited by low tumor induction rates until Matrigel augmentation was first described by our laboratory in 1998 [13, 15]. Initially, Matrigel augmentation was noted to induce tumors in 100% of mouse flanks, but this initial report was optimistic and our experience over the last 8 years places tumor induction closer to 60% (R.L. Jensen, personal observation) [13]. Furthermore, other investigators have not been able to replicate our tumor induction rates (R.L. Jensen, personal observation).

The purpose of this manuscript was to analyze our meningioma mouse flank tumor model to address two long-held criticisms: 1. Why are tumor induction rates so poor in animals injected with cell lines derived from operative specimens? 2. Are mouse flank tumors meningiomas? We reviewed our laboratory experience over the past three years with two immortal meningioma cell lines and cells derived from operative specimens in an attempt to address these criticisms.

MATERIALS AND METHODS

Analysis of Our Experience with the Meningioma Mouse Flank Model

Over the last three years our laboratory has used the mouse meningoma flank model to study the effects of various therapies on tumor growth (data not shown). The following report represents the control data from these *in vitro* and *in vivo* experiments. Consequently, not all operative specimens grown *in vitro* were processed for all experiments or implanted into the flanks of mice for *in vivo* studies.

UU IR Author Manuscript

Meningioma Surgical Specimens

Meningioma surgical specimens were obtained under a University of Utah Institutional Review Board (IRB) protocol and processed for immunohistochemistry and cell culture as described below. Tumors were graded according to World Health Organization criteria [21]. Patient data for *in vitro* and *in vivo* studies are listed in Table 1. In this paper, we will use the term "benign meningioma" to describe a WHO grade I meningioma and "primary cell line" to refer to newly established cell lines established from operative samples [21].

Meningioma Cell Culture

Tumor specimens were obtained from patients harboring meningiomas and grown as monolayer as described previously [12, 14]. Briefly, operative specimens were taken immediately from the operating room, digested in collagenase, and placed in Dulbecco's Modified Eagle Medium (DMEM) (Sigma) supplemented with 10% fetal calf serum, L-glutamine (2 μM), penicillin (50 IU/mL), and streptomycin (50 mg/mL). Cultured cells were maintained at 37°C in 7.5% CO_2. Only passages 1-5 were used in experiments for this study.

The human immortal cell lines IOMM-Lee and CH-157 MN were also grown in DMEM supplemented with 10% fetal calf serum, L-glutamine (2 μM), penicillin (50 IU/mL), and streptomycin (50 mg/mL) at 37°C in 7.5% CO_2 [18, 36]. The IOMM-Lee and CH-157 MN cell lines were kind gifts from Dr. Ian McCutcheon (University of Texas,

UU IR Author Manuscript

M.D. Anderson Cancer Center, Houston, Texas) and Dr. Yancey Gillespie (University of Alabama School of Medicine, Birmingham, Alabama), respectively.

Karyotyping: G-Band Chromosome Analysis

The meningioma cell lines were grown in T-175 flasks to confluence and processed by the cytogenetics core facility at the University of Utah for Giemsa-band chromosome analysis.

Cell Counts by Bright-line Hemocytometer

Cell lines were plated into 6 well plates at a density of $1x10^4$ or $1x10^5$ per well. Cell counts were accomplished each day (days 1–14) by harvesting the cells with trypsin and counting them using a bright-line hemocytometer. Cells in two wells were counted for each time point and two counts were done per well for a total of four counts per time point. Doubling times were calculated during logarithmic growth.

Fluorescent Activated Cell Sorting (FACS) for Cell-Cycle Phase

IOMM-Lee, CH-157 MN, and meningioma cell lines derived from operative specimens were plated in T-175 flasks (immortal cell lines $1x10^6$ cells per flask and operative cell lines $1x10^7$ cells per flask) at 30% confluence and allowed to grow for 24 hours to ensure logarithmic growth. Cells were harvested using Accutase (MP Biomedicals, Irvine, CA) and declumped by drawing them through a 26-gauge needle five times. Cells ($1x10^7$) were resuspended in 1 mL of ice-cold Dulbecco's phosphate-buffered saline (DPBS) and fixed by adding 2 mL of ice-cold methanol, then stored at

UU IR Author Manuscript

4°C for at least 2 hours. Cells are then rehydrated for 5 minutes in DPBS on ice and stained in 1 mL of DPBS/propidium iodide solution (50 µg/ml propidium iodide, 200 µg/ml RNase A, 0.1% Triton X-100) for 30 minutes in the dark at room temperature. The cells were sorted within 5 hours of staining by FACScan Analyzer (Becton-Dickinson, Franklin lakes, NJ) and results were analyzed using CellQuest (Becton-Dickinson).

Mouse Xenograft Flank Model: Transplanting and Harvesting Tumors

Cells were grown to confluence in T-175 flasks. All steps were carried out on ice. T-175 flasks were rinsed with PBS, trypsinized, counted, and pelleted at 1000 rpm for 5 minutes at 4ºC. Excess medium was removed and the pellet was resuspended in medium to obtain between $5.0x10^5$ and $1.5x10^6$ cells per mL for the IOMM-Lee cell line, between $1.0x10^6$ and $1.25x10^6$ cells per mL for the CH-157 MN cell line, and as many cells as were present in a T-175 flask for primary meningioma cell lines (cell counts for patients #3, #4, #5, and #6 are $1.6x10^7$, $1.1x10^7$, $1.0x10^5$, and $1.7x10^6$ cells per flank, respectively). One-milliliter aliquots were placed in 2-mL microtubes and spun at 1,000 rpm for 5 minutes at 4ºC. Excess media was removed and the tumor cells were resuspended and aspirated into 1-cc tuberculin syringes. For the IOMM-Lee and CH-157 MN cell lines, 0.5 mL of media was used to resuspend the pellet before aspiration into the tuberculin syringe. For primary meningioma cell lines, 0.5 mL of Matrigel (B.D. Biosciences, Bedford, MA) was used to resuspend the pellet before aspiration into the tuberculin syringe. Tumor cells were injected subcutaneously into the flanks of 3-week-old immunodeficient mice (CD1, Charles River Laboratories, Wilmington, MA) using a 25-gauge needle. A total of 20 mice were injected with the IOMM-Lee cell line (5 mice x

UU IR Author Manuscript

4 experiments) and 10 mice with the CH-157 MN cell line (5 mice x 2 experiments). Five animals each were injected with cell lines derived from patients #3, #4, #5, and #6. Biweekly caliper measurements are started 10–14 days after injection to give time for the media or Matrigel to resorb completely.

Mice were sacrificed with a lethal intraperitoneal injection of pentobarbital. Flank tumors were excised, cut into blocks, and placed in 10% formalin for paraffin blocks or in 2.5% paraldehyde and 1% glutaraldehyde for electron microscopy.

Survival Analysis

Survival curves were graphed by analyzing the number of mice surviving until sacrifice (Comparison of Survival Curves, GraphPad Prism 4.0, San Diego, CA). Animals were sacrificed because of large tumor size.

Immunohistochemical Staining for Vimentin, Epithelial Membrane Antigen (EMA), Glial Fibrillary Acidic Protein (GFAP), and MIB-1

Immunohistochemical stainings were performed by ARUP Laboratories (Salt Lake City, Utah). Briefly, slides were cut at 4 microns, then melted at 55–60°C for 30 minutes, deparaffinized in xylene for 5 minutes, and rehydrated in graded alcohols (100% x 2, 95% x 2, 70% x 1) for 1 minute each. The following steps were performed on the Ventana ES (Ventana Medical Systems, Tucson, AZ) at 40°C. Heat-induced epitope retrieval was applied in citrate buffer (pH 6.0) in a microwave oven for 15 minutes at half power and allowed to cool for 15 minutes for tissue stained for vimentin, EMA, and GFAP. For the MIB-1 immunohistochemical staining, heat-induced epitope retrieval was

UU IR Author Manuscript

applied in citrate buffer (pH 6.0) in an electric pressure cooker for 3 minutes and allowed to cool for 27 minutes. The primary antibodies were applied for 32 minutes [Vimentin (1:300, mouse monoclonal Ab, Clone Vim 3B4, Dako Cytomation, Carpinteria, CA), EMA (1:200, mouse monoclonal Ab, Clone E29, Dako Cytomation), GFAP (1:400, mouse monoclonal Ab, Clone 6F2, Dako Cytomation), Ki-67 (1:100, mouse monoclonal Ab, Clone MIB-1, Dako Cytomation), Factor 8 (1:1600, rabbit polyclonal Ab, Dako Cytomation)] followed by the appropriate secondary antibody for 8 minutes [Human Tissue: Goat anti-mouse/anti-rabbit (1:300, Rabbit Fab, Dako Cytomation); Mouse Tissue: Mouse Fab (1:200, Mouse IgG, Dako Cytomation)]. Detection was done using the IView DAB detection kit (Ventana) and the counterstain was done with Hematoxylin (Ventana) for 4 minutes. Slides were then dehydrated through graded alcohols (70% x 1, 95% x 2, 100% x 2) for 30 seconds each, dipped in 4 changes of xylene, and covered with a coverslip. Positive controls consisted of normal uterus, normal pancreas, pancreas tumor, and normal tonsil for vimentin, EMA, MIB-1 and factor 8, respectively. Negative controls were accomplished by running the above positive control tissue without the primary antibody.

MIB-1 Immunohistochemical Analysis

Analysis of MIB-1 staining was performed by taking 6 random pictures per slide at 400X (10 ocular x 40 objective) using an Olympus Microfire camera. The images were analyzed using the Image-Pro Plus 5.0 graphic analysis program (Media Cybernetics, Silver Spring, MD). Results were reported as number of MIB-1 cells positive per 40x high-powered-field (hpf) and represent the mean (±S.D.) of 6 random

UU IR Author Manuscript

fields per slide. Two slides were analyzed per original operative sample (i.e., 12 total data points). For meningioma flank tumors one slide was analyzed per animal, three animals per group (i.e., 18 total data points).

Transmission Electron Microscopy (TEM)

Operative and mouse tumor samples were harvested, cut into 1-mm^3 blocks, and fixed in 2.5% paraformaldehyde with 1% glutaraldehyde. Cell culture meningiomas were grown to confluence in T-175 flasks, rinsed with PBS, scraped, pelleted, and fixed in 2.5% paraformaldehyde with 1% glutaraldehyde. After at least 24 hours of fixation, samples were rinsed twice for 10 minutes each, in 0.1M sodium cacodylate buffer with sucrose and calcium chloride at pH 7.4. This was followed by post-fixing in 2% osmium tetroxide in 0.1M sodium cacodylate buffer for 45 minutes at room temperature on a rotator. Samples were then rinsed in distilled water for 5 minutes and stained en bloc in aqueous uranyl acetate for 45 minutes at room temperature on a rotator. Samples were then dehydrated with increasing alcohol concentrations (50%–100%) at room temperature on a rotator. Cells were then infiltrated with and then embedded in Spurr's plastic. Thin sections were cut on a Leica UCT Ultramicrotome with a Diatome diamond knife, stained with uranyl acetate and Reynolds's lead citrate, and examined on a Hitachi H 7100 TEM at 75 KV. Photographs were taken on Kodak 4489 film.

RESULTS

Meningioma Characteristics

UU IR Author Manuscript

Tumors were taken from 9 patients for establishment of primary cell cultures and the immortal cell lines IOMM-Lee and CH-157 for a total of 11 cell cultures. Of these 11 patients, 73% were women; the age range of the patients was from 38 to 71 years with a median of 53 years (Table 1) [18, 36]. Intracranial meningoma location in the patients varied, as did the meningoma subtypes (although 6 were benign transitional tumors) (Table 1).

G-Band Karyotyping

Giemsa-band karyotyping was achieved on both immortal cell lines and six primary meningioma cell lines (Table 1). G-band analysis exhibited three general karyotypes: normal, a single chromosomal abnormality, or multiple chromosomal abnormalities. We grouped these further into simple and complex chromosomal karyotypes. Simple karyotypes were defined as normal or only one chromosomal abnormality, whereas complex karyotypes were meningiomas exhibiting multiple chromosomal abnormalities (Figure 1). Karyotyping of the IOMM-Lee cell line showed a complex karyotype with multiple chromosomal abnormalities fitting its initial description in 1990 (Table 1) [18]. The CH-157 MN cell line also exhibited a complex karyotype (Table 1). Both immortal cell lines showed additions to chromosomes 2, 5, 12, and 14 with loss of chromosome 17 (Table 1). Complex karyotypes were also seen in patients 3, 4, and 8, with similar chromosomal abnormalities noted on chromosomes 4, 5, 6, 9, and 12 (Table 1). Simple karyotypes were seen with patient 6 (monosomy 22, Table 1) and patients 5 and 7 (normal karyotypes, Table 1).

UU IR Author Manuscript

In vitro Growth Rates

The *in vitro* growth rates of 6 cell lines were analyzed. Immortal meningioma cell lines showed the fastest *in vitro* growth rates, with doubling times of 20 and 23 hours, for IOMM-Lee and CH-157 MN cell lines, respectively (Figure 2). Meningiomas cultivated from operative specimens were noted to fall into fast- and slow-growing groups (Figure 2). Fast-growing cell lines were derived from patients 3 and 4, with doubling times of 40 and 65 hours, respectively (Figure 2). Slower-growing cell lines were obtained from patients 5 and 7, with doubling times of ~120 hours (Figure 2). Interestingly, faster-growing cell lines had complex karyotypes (IOMM-Lee, CH-157 MN, patients 3 and 4), whereas slower-growing cell lines were derived from cell cultures exhibiting a simple karyotype (i.e., patients 5 and 7). Unlike the immortal cell lines, all cell lines cultivated from our operative specimens showed contact inhibition, slowing their growth rates as they reached confluence. Plating efficiency for the immortal cell lines was greater than 90%, whereas plating efficiency of cell lines obtained from operative specimens ranged from 40–90% and was dependent on trypsinization times; improved plating efficiency was seen with lower trypsin times.

FACS for Cell-Cycle Phase

Flow cytometry for cell cycle characteristics was obtained on 7 cell lines growing logarithmically *in vitro* (IOMM-Lee, CH-157 MN, patients 4, 5, 8, 9, and 11) (Figure 3). The mean (±S.D.) percentage of IOMM-Lee cells in gap 1 (G1), synthesis (S) and gap 2 (G2) was 40%±3%, 37%±8%, and 23%±7%, respectively. The CH-157 MN cell line

UU IR Author Manuscript

exhibited 58%±5%, 38%±2%, and 4%±3% of cells in G1, S, and G2 phase, respectively.

The cell lines derived from operative specimens showed between 44% and 62% of cells in G1, 17% to 32% of cells in S, and 11% to 39% of cells in G2. Overall, the immortal cell lines IOMM-Lee and CH-157 MN showed greater than 35% percent of cells in S phase, whereas the percentage of cells in S phase of operative cell cultures was lower (Figure 3).

Mouse Flank Tumor Growth Rates and Survival Proportions

A total of six cell lines were implanted into the flanks of nude mice, four cell lines with a complex karyotype (IOMM-Lee, CH-157 MN, patients 3 and 4) and two cell lines with a simple karyotype (patients 5 and 6) (Figure 4). The IOMM-Lee cell line induced flank tumors in 95% (19/20) of animals after subcutaneous injection of $5.5x10^5$–$1.4x10^6$ cells per flank. Four of 20 (20%) animals died from tumor involvement. At autopsy, all four animals showed severe abdominal ascites with tumors invading through the abdominal peritoneum. Large organ metastases (e.g., lung, liver, kidney, and intestines) were not noted. Animal death was believed to be from compromise of the abdominal peritoneum with weeping of serous fluid into the abdominal cavity. All animals were sacrificed at 56 days because of tumor size. Mean tumor volumes (mm^3) (±S.D.) at 15, 29, 43, and 56 days were 457 ± 347 mm^3, 1228 ± 782 mm^3, 2353 ± 1258 mm^3, and 4593 ± 1377 mm^3, respectively (Figure 4).

UU IR Author Manuscript

The CH-157 MN cell line induced flank tumors in 100% (10/10) of animals after subcutaneous injection of $1.1x10^6$–$1.2x10^6$ cells per flank. All animals survived to 43 days and were sacrificed because of tumor size per animal protocol. Mean tumor volumes (mm^3) (±S.D.) at 15, 29, and 43 days were 82 ± 46 mm^3, 819 ± 654 mm^3, and 3196 ± 2574 mm^3, respectively (Figure 4).

Two complex karyotype meningioma cell lines (Patients 3 and 4) showed excellent flank tumor induction and growth. The cell line from patient 3 induced tumors in 100% (5/5) of animals after subcutaneous injection of $1.6x10^7$ cells per animal flank, with Matrigel. All mice survived. Animals were sacrificed at 35 days because of tumor size per animal protocol. Mean tumor volumes (±S.D.) at 14, 24, and 35 days were 3038 ± 800 mm^3, 5304 ± 1343 mm^3, and 7473 ± 2694 mm^3, respectively (Figure 4). The cell line derived from patient 4 also induced tumors in 100% (5/5) of animals after subcutaneous injection of $1.1x10^7$ cells per animal flank. One animal died at 28 days because of tumor involvement. At autopsy, significant abdominal ascites was noted with tumor invading through the abdominal peritoneum. No metastasis of large organs (e.g., lung, liver, colon, or kidney) was noted. The cause of death was presumed to be similar to that it the IOMM-Lee animals, with serous exudate of the tumor into the abdominal cavity. Animals were sacrificed at 35 days because of tumor size, per animal protocol. Mean tumor volumes (±S.D.) at 14, 24, and 35 days were 2080 ± 872 mm^3, 3053 ± 1260 mm^3, and 5588 ± 3405 mm^3, respectively (Figure 4).

Two simple karyotype meningioma cell lines (patient 5 and 6) were transplanted into mice and followed for a period of 2–3 months, during which the implanted tumors which did not grow (i.e., small tumors without growth). Flank tumors incited from simple

UU IR Author Manuscript

karyotypes showed tumor take, but no significant growth after injection of $1.0x10^5$ cells and $1.7x10^6$ cells per flank for patients 5 and 6, respectively. Histologic analysis of flank tumors from patient 6 showed meningoma tumor cells (see below).. All mice survived. Animals were sacrificed at 96 days and 51 days for lack of tumor growth from patients 5 and 6, respectively (Figure 4).

Mouse Flank Tumor Histology and Immunohistochemical Staining Results

Mouse flank tumors were processed for hematoxylin and eosin (H&E) staining, as well as immunohistochemically for GFAP, vimentin, EMA, and MIB-1. Both immortal cell lines showed hypercellular sheets without whorl formation and stained positive for vimentin, negative for GFAP, and weakly positive for EMA (Table 2, Figure 5). These flank tumors exhibited a high number of MIB-1–positive cells (Figure 5). The IOMM-Lee tumor invaded soft tissue, whereas the CH-157 MN cell line did not, but both exhibited a central core of necrosis.

Flank tumors induced by meningiomas with complex karyotypes (patients 3 and 4) induced large tumors that showed lobular growth patterns with prominent nuclei, resembling their original operative specimens on H&E staining (Figure 5). The tumor induced by meningiomas from patient 3 showed features of a meningothelial meningoma in both the operative and flank tumor specimen (data not shown). Immunohistochemically, the tumors induced from the meningiomas in patients 3 and 4 showed similar results when operative specimens were compared with their corresponding flank tumor: they were GFAP negative, vimentin positive, with weak EMA

UU IR Author Manuscript

staining (Table 2, Figure 5). MIB-1 stainings of the operative samples showed significant proliferative rates.

Mouse flank tumors grown from meningioma cell cultures with a simple karyotype (patients 5 and 6) showed no significant tumor growth (i.e., non-growing tumors). Histologic analysis of the non-growing tumors from patient 6 showed the characteristic whorls and cell rests of a transitional meningioma, unlike the original operative specimen, which exhibited fibrous meningoma features of parallel spindle cells with wide fascicles (Figure 5). The operative MIB-1 staining showed many positive cells, whereas none were observed in the flank tumor sample. Moderate and weak vimentin immunostaining was noted in the operative and flank tumor specimens.

MIB-1 Counts

MIB-1 immunohistochemical staining data represents the mean number of positive cells per high-powered-field (hpf) ±S.D. (Figure 6). The original operative specimens for the immortal cell lines were unavailable for analysis. The two operative specimens that induced mouse flank tumors showed MIB-1 counts of 5.7 ± 4.1 and 1.1 ± 1.1 for patients 3 and 4, respectively. The two operative specimens that showed tumor regression showed MIB-1 counts of 1.9 ± 1.3 and 13.6 ± 6.8, for patients 5 and 6, respectively. Analysis of cell lines inciting meningoma flank tumors showed MIB-1 counts of ~200 per hpf (211.0 ± 75.7, 190.6 ± 23.8, 243.9, ± 30, 232.7 ± 60, for IOMM-Lee, CH-157 MN, and cell lines from patients 3 and 5, respectively). Of the two primary cell lines from simple karyotypes, only one (patient 6) was processed for analysis. This

UU IR Author Manuscript

cell line showed no cells positive for MIB-1 immunoreactivity. Interestingly, we observed that MIB-1 counts from operative specimens did not predict the ability to incite flank tumor growth. For example, patient 4 had the lowest MIB-1 mean but consistently incited flank tumors, whereas patient 5 had the highest MIB-1 ratio but incited nongrowing tumors (Figure 6).

TEM

TEM was used to identify ultrastructural features consistent with the diagnosis of meningiomas, specifically desmosomes. Desmosomes are intercellular junctions that anchor vimentin filaments to the cellular membrane and are characteristic of meningiomas. The key features of desmosomes are opposing disc-shaped plaques located on the cytoplasmic membrane, with inserting cytoplasmic tonofilament bundles, and an amorphous material present within the intercellular space (Figure 7). Four cell lines, three flank tumors, and one operative sample were processed for TEM. Ultrastructural features of the IOMM-Lee cell line include interdigitating cells with prominent nucleoli and intermediate filaments. Microvilli were noted on the cellular surface. Tight junctions (i.e., no intervening intercellular space) and junctions suggestive of desmosomes (i.e., intercellular gap with shaggy appearance to lipid bilayer) were visualized. These features still fit its initial description in 1990 [18]. Ultrastructurally, primary meningiomas grown in cell culture (from patients 4, 8, and 11) exhibited interdigitating cell processes without intercellular junctions. Flank tumors induced by the IOMM-Lee, CH-157 MN, and patient 5 cell lines were processed for TEM. The IOMM-Lee and CH-157 MN mouse flank tumors exhibited junctional complexes similar in

UU IR Author Manuscript

appearance to desmosomes but lacking clear cytoplasmic tonofilament insertion (Figure 7). The mouse flank tumor induced from the patient 5 cell line exhibited clear desmosomes (Figure 7).

DISCUSSION

This manuscript addresses two long-held criticisms of the mouse meningoma flank model: 1. Why are tumor induction rates so poor in animals injected with cell lines derived from operative specimens? 2. Are mouse flank tumors meningiomas? The advantages to the mouse xenograft meningioma flank model are the ease with which tumors can be continually assessed during treatments and the relatively low cost of using mice as an animal model. Historically, the meningioma mouse flank model was limited by low tumor induction rates until Matrigel augmentation was first described in reports from our laboratory in 1998 [13, 15]. Initially, Matrigel augmentation was noted to induce tumors in 100% of mouse flanks, but this initial report was optimistic and our experience over the last 8 years places tumor induction closer to 60% (R.L. Jensen, personal observation) [13]. Furthermore, other investigators have had little success in duplicating our model (R.L. Jensen personal conversations). In this analysis, we identified that meningiomas grown in culture containing multiple chromosomal abnormalities consistently induced flank tumors, whereas normal cultures or those with a single chromosomal abnormality did not. Finally, flank tumors derived from both immortal cell lines and operative specimens exhibit histologic, immunohistochemical and ultrastructural features consistent with meningiomas.

UU IR Author Manuscript

A Complex Karyotype Appears to Predict the Successful Growth of Meningiomas in Mouse Flanks

In this study, the chromosomal abnormalities exhibited are consistent with previously reported meningoma chromosomal abnormalities [29]. Cytogenetic and molecular studies have identified loss of heterozygosity of chromosome 22 in roughly 60% of all meningiomas, with the *NF2* tumor suppressor gene, located on chromosome 22q12.1, and its protein product (i.e., schwannomin or Merlin) noted to be dysfunctional or lost in approximately one third of meningoma cases [4, 9, 19, 20, 29, 33, 42, 43]. Many other cytogenetic alterations have been identified and associated with atypical or anaplastic histology, including the presence of dicentric or ring chromosomes and losses of chromosome arms 1p, 6q, 7, 9p, 10, 14q, 18q, 19, or 20, as well as gains/amplifications of 1q, 9q, 12q, 15q, 17q, or 20q [3, 5, 7, 8, 16, 17, 19, 27, 28, 32, 34, 39, 41]. The immortal cell lines IOMM-Lee and CH-157 MN showed chromosomal abnormalities consistent with cell lines passaged multiple times. Meningiomas from operative samples fell into two groups: those with complex and those with simple karyotypes. The three meningiomas with a complex karyotype (patients 3, 4, and 8) had similar abnormalities, despite being from three different meningioma subtypes (meningothelial, transitional, and psammomatous). All three exhibited additions to chromosomes 4, 6, 9, and 12 and deletions of chromosome 5. Meningiomas with a simple karyotype exhibited either a normal chromosomal number (patients 5 and 7) or monosomy 22 (patient 6). Interestingly, cell lines with the complex karyotype grew quickly in culture and were able to induce mouse flank tumors.

UU IR Author Manuscript

Cell cultures derived from complex karyotypes exhibited faster growth rates *in vitro* and consistently induced fast-growing mouse flank tumors. It is unclear whether tumor induction was simply a function of the initial cell burden injected subcutaneously into the flanks of nude mice, since meningiomas with multiple chromosomal abnormalities grew quickly in culture; a much greater cellular harvest was obtainable by the fifth passage, the arbitrary cut-off that we set for subcutaneous injection. It is the authors' belief that meningiomas with multiple chromosomal abnormalities act more aggressively because of unknown gene dysregulation that is not present in meningiomas with simple karyotypes.

Interestingly, we observed that MIB-1 counts from operative specimens did not predict the ability to incite flank tumor growth (e.g., patient 4 had the lowest MIB-1 mean but consistently incited flank tumors, whereas patient 5 had the highest MIB-1 ratio but only incited non-growing flank tumors). Induced mouse tumors showed significant MIB-1 counts with >30% of cells stained positive, indicating high proliferative rates. Others have reported MIB-1 index of intracranial IOMM-Lee tumors to be 30% [40].

The Meningioma Mouse Xenograft Flank Model Recapitulates the Histologic, Immunohistochemical, and Ultrastructural Features of Meningiomas

All meningiomas grown in mouse flanks showed histologic, immunohistochemical, and ultrastructural features consistent with meningiomas. Previous work has characterized meningiomas grown *in vitro* on a microscopic, immunohistochemical, and ultrastructural level [12, 14, 31]. These studies conclude that cell cultures derived from meningioma operative samples appear to be of

UU IR Author Manuscript

leptomeningeal origin. This conclusion is based on their polygonal shape, negative GFAP staining, and positive vimentin and EMA staining, as well as the exhibition of desmosomes by electron microscopy [12, 31]. Low-passage cells (no greater than passage 5) were used for these experiments, making fibroblast overgrowth less likely. Finally, cell lines used for *in vitro* work were transplanted into the flanks of nude mice for *in vivo* experiments, and the xenograft tumors that developed resembled meningiomas histologically, immunohistochemically, and ultrastructurally.

Histologically, meningiomas grown in the mouse flank shared a histologic features similar to that of the original operative specimen (e.g., immortal cell lines exhibited cytoarchitecture of WHO grade III meningoma with nuclear polymorphism and numerous mitosis and flank tumors from operative specimens showed lobular cellular patterns similar to their original operative specimens) (Figure 5). Immunohistochemically, the hallmark of meningiomas is vimentin positive staining and negative GFAP staining, with roughly 80% staining for EMA. Mouse flank tumors grown from meningioma cell culture showed 100% vimentin immunoreactivity. In this analysis all flank tumors exhibited similar immunohistochemical stainings as the original operative specimen, with the exception of patient 6, which lost EMA reactivity in the flank tumor. Finally, ultrastructurally meningiomas grown in mouse flanks exhibited desmosomes, as well as junctional complexes consistent with meningiomas.

Ultrastructural Features of Meningiomas

Desmosomes are intercellular junctions characteristic of meningiomas and arachnoidal tissue [1]. Three molecular features are typical of meningiomas: vimentin,

EMA, and desmosomes [1]. Desmosomes are unique to meningiomas and are not exhibited in other primary intracranial tumors [1]. Arachnoidal and meningioma desmosomes anchor vimentin filaments to the cytoplasmic membrane. Typical ultrastructural features of meningiomas include flat and often interdigitating cell processes, desmosomal structures, and loosely arranged vimentin filaments, the amount of which strongly varies [1]. Cell processes and larger areas of cell bodies densely packed with intermediate filaments were adjacent to cells with only rare intermediate filament networks [1]. In addition to desmosomes, two other types of intercellular junctions have been described in meningiomas [1]. One is characterized by cytoplasmic plaque structures, smaller and less dense than those of desmosomes, and without intermediate filament association often formed by the approach of three cellular extensions. These intercellular junctions with diffuse cytoplasmic plaques and no associated intermediate filaments are frequently found in meningiomas, as well as intercellular structures with a pentilaminar appearance [1]. The other intercellular contact was formed by the direct attachment of neighborhood plasma membranes, forming a pentilaminar structure [1].

Dr. Wei-Hwa Lee first described his intraosseous malignant meningioma cell line (IOMM-Lee) in 1990 and electron microscopy shows ultrastructural features that still fit its initial description of prominent nucleoli, intermediate filaments, and sparse microvilli on the cellular surface [18]. When the IOMM-Lee cell line was grown *in vivo* and examined with electron microscopy, we identified intercellular junctional complexes consistent with meningiomas (Figure 7). The CH-157 MN cell line grown in mouse

UU IR Author Manuscript

flanks also exhibited similar junctional complexes. One operative specimen grown *in vivo* (patient 5) exhibited desmosomes.

Recommendations for Inducing Meningioma Mouse Flank Tumors

Induction of flank tumors from the immortal cell lines IOMM-Lee and CH-157 MN can be successfully accomplished by injecting $1x10^6$ cells suspended in 0.5 mL of media subcutaneously into the flanks of nude mice. One T-175 flask contains enough cells to inject approximately 30 mouse flanks. In our experience, therapies should be instituted 5–10 days after injection, because these tumors appear to "take off" around two weeks. Waiting longer to institute therapies makes it difficult to separate growth curves.

Induction of flank tumors using primary meningoma cell lines should be undertaken with cell lines that are identified either to contain multiple chromosomal abnormalities or to grow quickly in cell culture with doubling times of less than 3 days (72 hours). The number of cells injected per flank should range from $5x10^6$ to $1x10^7$ and be suspended in 0.5 mL of Matrigel. Although higher cell numbers were injected in these experiments, these tumors grew too quickly and lowering the initial cell burden would aid in decreasing the rapid growth. Treatment should be instituted between 10 and 14 days after injection to allow for Matrigel resorption. Slow-growing meningoma cell lines with doubling times greater than 3 days or simple karyotypes are not amenable for inducement of subcutaneous flank tumors.

CONCLUSIONS

UU IR Author Manuscript

Meningioma cell cultures with multiple chromosomal abnormalities consistently induce mouse flank tumors. The meningoma mouse xenograft model recapitulates the histologic, immunohistochemical, and ultrastructural features present in meningiomas.

ACKNOWLEDGMENTS

We thank Kristin Kraus for her excellent editorial assistance, Nancy B. Chandler for her electron microscopy expertise, and Sheryl Tripp for her immunohistochemical staining expertise. This work was supported in part by a grant from the American Association of Neurological Surgeons Neurosurgery Research and Education Foundation to Brian Ragel.

UU IR Author Manuscript

REFERENCES

1. Akat K, Mennel HD, Kremer P, et al. Molecular characterization of desmosomes in meningiomas and arachnoidal tissue. Acta Neuropathol (Berl) 2003;106:337-347.
2. Al-Rodhan RF, Laws ER. The History of Intracranial Meningiomas. In: Al-Mefty O, ed. Meningiomas. New York: Raven Press, Ltd.; 1991:1-6.
3. Al Saadi A, Latimer F, Madercic M, et al. Cytogenetic studies of human brain tumors and their clinical significance. II. Meningioma. Cancer Genet Cytogenet 1987;26:127-141.
4. Bigner SH, Mark J, Bigner DD. Cytogenetics of human brain tumors. Cancer Genet Cytogenet 1990;47:141-154.
5. Bostrom J, Meyer Puttlitz B, Wolter M, et al. Alterations of the tumor suppressor genes CDKN2A (p16(INK4a)), p14(ARF), CDKN2B (p15(INK4b)), and CDKN2C (p18(INK4c)) in atypical and anaplastic meningiomas. Am J Pathol 2001;159:661-669.
6. Burger PC, Scheithauer BW, Vogel FS, eds. Surgical Pathology of the Nervous System and Its Coverings. Fourth ed. Philadelphia: Churchhill Livingstone; 2002.
7. Cai DX, Banerjee R, Scheithauer BW, et al. Chromosome 1p and 14q FISH analysis in clinicopathologic subsets of meningioma: diagnostic and prognostic implications. J Neuropathol Exp Neurol 2001;60:628-636.
8. Cai DX, James CD, Scheithauer BW, et al. PS6K amplification characterizes a small subset of anaplastic meningiomas. Am J Clin Pathol 2001;115:213-218.

UU IR Author Manuscript

9. Dumanski JP, Rouleau GA, Nordenskjold M, et al. Molecular genetic analysis of chromosome 22 in 81 cases of meningioma. Cancer Res 1990;50:5863-5867.

10. Gonzales MF. Classification of brain tumors. In: Kaye AH, Laws ER, eds. Brain Tumors. 1st ed. Edinburgh: Churchill Livingstone; 1995:675.

11. Greene HS, Arnold H. The homologous and heterologous transplantation of brain and brain tumors. J Neurosurg 1945;2:315-329.

12. Jensen RL, Lee YS, Guijrati M, et al. Inhibition of in vitro meningioma proliferation after growth factor stimulation by calcium channel antagonists: Part II--Additional growth factors, growth factor receptor immunohistochemistry, and intracellular calcium measurements. Neurosurgery 1995;37:937-946; discussion 946-947.

13. Jensen RL, Leppla D, Rokosz N, et al. Matrigel augments xenograft transplantation of meningioma cells into athymic mice. Neurosurgery 1998;42:130-135; discussion 135-136.

14. Jensen RL, Origitano TC, Lee YS, et al. In vitro growth inhibition of growth factor-stimulated meningioma cells by calcium channel antagonists. Neurosurgery 1995;36:365-373; discussion 373-374.

15. Jensen RL, Wurster RD. Calcium channel antagonists inhibit growth of subcutaneous xenograft meningiomas in nude mice. Surg Neurol 2001;55:275-283.

16. Katsuyama J, Papenhausen PR, Herz F, et al. Chromosome abnormalities in meningiomas. Cancer Genet Cytogenet 1986;22:63-68.

UU IR Author Manuscript

17. Lamszus K, Kluwe L, Matschke J, et al. Allelic losses at 1p, 9q, 10q, 14q, and 22q in the progression of aggressive meningiomas and undifferentiated meningeal sarcomas. Cancer Genet Cytogenet 1999;110:103-110.

18. Lee WH. Characterization of a newly established malignant meningioma cell line of the human brain: IOMM-Lee. Neurosurgery 1990;27:389-395; discussion 396.

19. Lekanne Deprez RH, Bianchi AB, Groen NA, et al. Frequent NF2 gene transcript mutations in sporadic meningiomas and vestibular schwannomas. Am J Hum Genet 1994;54:1022-1029.

20. Leon SP, Zhu J, Black PM. Genetic aberrations in human brain tumors. Neurosurgery 1994;34:708-722.

21. Louis DN, Scheithauer BW, Budka H, et al., eds. Meningiomas. Lyon: IARC Press; 2000. Kleihues P, Cavenee WK, eds. World Health Organization Classification of Tumours: Pathology and Genetics: Tumours of the Nervous System.

22. Mahmood A, Caccamo DV, Tomecek FJ, et al. Atypical and malignant meningiomas: a clinicopathological review. Neurosurgery 1993;33:955-963.

23. Martuza RL, Malick A, Markert JM, et al. Experimental therapy of human glioma by means of a genetically engineered virus mutant. Science 1991;252:854-856.

24. McCutcheon IE, Friend KE, Gerdes TM, et al. Intracranial injection of human meningioma cells in athymic mice: an orthotopic model for meningioma growth. J Neurosurg 2000;92:306-314.

UU IR Author Manuscript

25. Medhkour A, Van Roey M, Sobel RA, et al. Implantation of human meningiomas into the subrenal capsule of the nude mouse. A model for studies of tumor growth. J Neurosurg 1989;71:545-550.

26. Olson JJ, Beck DW, Schlechte JA, et al. Effect of the antiprogesterone RU-38486 on meningioma implanted into nude mice. J Neurosurg 1987;66:584-587.

27. Ozaki S, Nishizaki T, Ito H, et al. Comparative genomic hybridization analysis of genetic alterations associated with malignant progression of meningioma. J Neurooncol 1999;41:167-174.

28. Prempree T, Amornmarn R, Faillace WJ, et al. 1;19 translocation in human meningioma. Cancer 1993;71:2306-2311.

29. Ragel BT, Jensen RL. Molecular genetics of meningiomas. Neurosurg Focus 2005;19:E9.

30. Rana MW, Pinkerton H, Thornton H, et al. Heterotransplantation of human glioblastoma multiforme and meningioma to nude mice. Proc Soc Exp Biol Med 1977;155:85-88.

31. Rutka JT, Giblin J, Dougherty DV, et al. An ultrastructural and immunocytochemical analysis of leptomeningeal and meningioma cultures. J Neuropathol Exp Neurol 1986;45:285-303.

32. Schneider BF, Shashi V, von Kap herr C, et al. Loss of chromosomes 22 and 14 in the malignant progression of meningiomas. A comparative study of fluorescence in situ hybridization (FISH) and standard cytogenetic analysis. Cancer Genet Cytogenet 1995;85:101-104.

UU IR Author Manuscript

33. Seizinger BR, de la Monte S, Atkins L, et al. Molecular genetic approach to human meningioma: loss of genes on chromosome 22. Proc Natl Acad Sci U S A 1987;84:5419-5423.

34. Simon M, von Deimling A, Larson JJ, et al. Allelic losses on chromosomes 14, 10, and 1 in atypical and malignant meningiomas: a genetic model of meningioma progression. Cancer Res 1995;55:4696-4701.

35. Simpson D. The recurrence of intracranial meningiomas after surgical treatment. J Neurochem 1957;20:22-39.

36. Tsai JC, Goldman CK, Gillespie GY. Vascular endothelial growth factor in human glioma cell lines: induced secretion by EGF, PDGF-BB, and bFGF. J Neurosurg 1995;82:864-873.

37. Tsai JC, Hsiao YY, Teng LJ, et al. Regulation of vascular endothelial growth factor secretion in human meningioma cells. J Formos Med Assoc 1999;98:111-117.

38. Ueyama Y, Morita K, Ochiai C, et al. Xenotransplantation of a human meningioma and its lung metastasis in nude mice. Br J Cancer 1978;37:644-647.

39. Vagner Capodano AM, Grisoli F, Gambarelli D, et al. Correlation between cytogenetic and histopathological findings in 75 human meningiomas. Neurosurgery 1993;32:892-900; discussion 900.

40. van Furth WR, Laughlin S, Taylor MD, et al. Imaging of murine brain tumors using a 1.5 Tesla clinical MRI system. Can J Neurol Sci 2003;30:326-332.

UU IR Author Manuscript

41. Weber RG, Bostrom J, Wolter M, et al. Analysis of genomic alterations in benign, atypical, and anaplastic meningiomas: toward a genetic model of meningioma progression. Proc Natl Acad Sci U S A 1997;94:14719-14724.

42. Wellenreuther R, Kraus JA, Lenartz D, et al. Analysis of the neurofibromatosis 2 gene reveals molecular variants of meningioma. Am J Pathol 1995;146:827-832.

43. Wolff RK, Frazer KA, Jackler RK, et al. Analysis of chromosome 22 deletions in neurofibromatosis type 2-related tumors. Am J Hum Genet 1992;51:478-485.

UU IR Author Manuscript

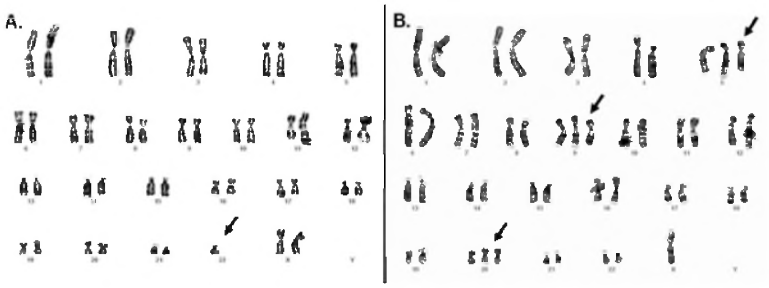

Figure 1: Representative Giemsa-band analysis of simple (A) and complex (B) karyotypes. A. Patient 6 showed a simple karyotype with monosomy 22 (arrow). B. Patient 4 exhibited a complex karyotype with multiple chromosomal abnormalities primarily involving chromosomes 1, 4, 5, 6, 9 and 12 (arrows).

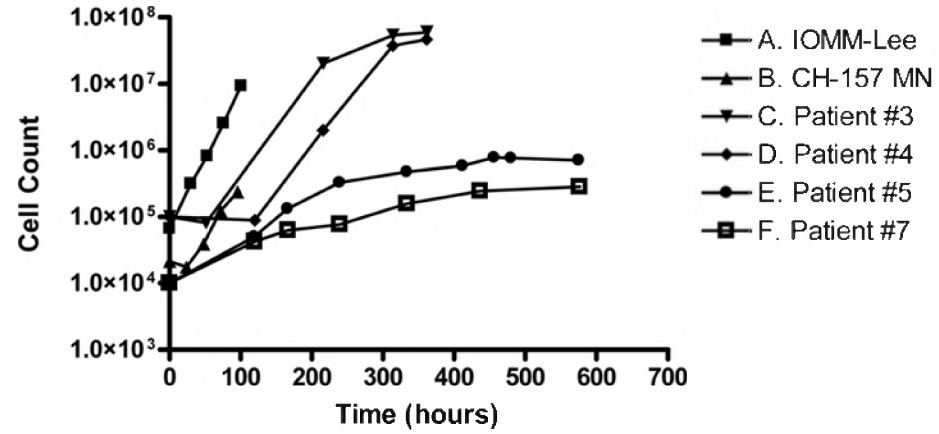

Figure 2: Logarithmic graph (Log10) comparing the *in vitro* growth rates of immortal cell lines (A–B) and benign meningiomas cultivated from operative samples (C–F, Table 1, Patients 3, 4, 5, and 7). The IOMM-Lee (A) and CH-157 MN (B) malignant cell lines showed doubling times of ~20 and ~23 hours, respectively. Cultures obtained from operative specimens fell into fast- and slow-growing groups (C–F). Faster-growing cell lines were from patients 3 and 4 (C–D) with doubling times of ~40 and ~65 hours,

UU IR Author Manuscript

respectively. Cell lines from patients 5 and 7 (E–F) showed slower growth with doubling times of ~120. Note: Operative specimens exhibited contact inhibition with slowing of their growth rates as they reached confluence, unlike the immortal cell lines. Error bars represent standard deviation (±S.D).

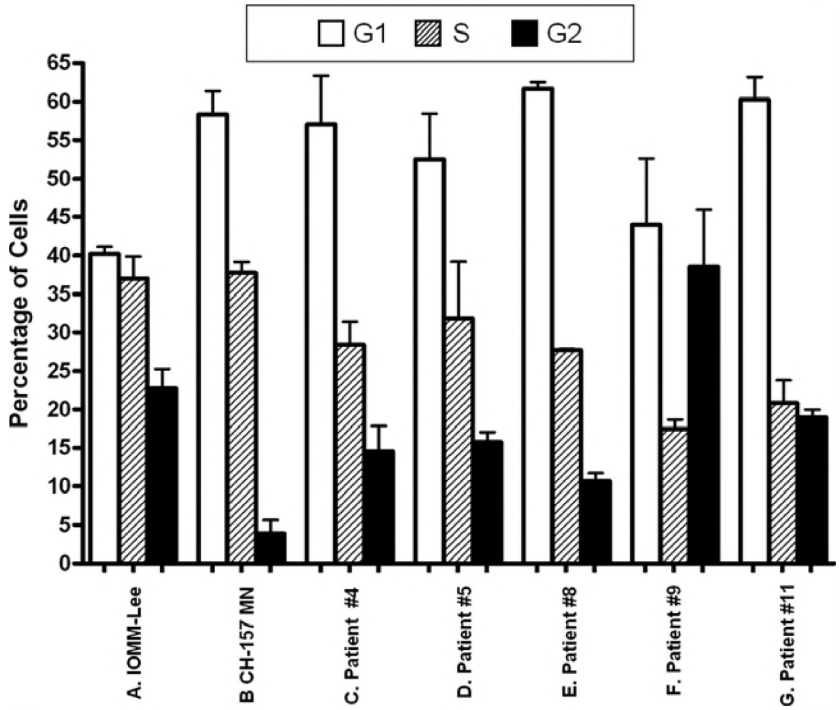

Figure 3: Flow cytometry cell cycle characteristics of logarithmic growing meningoma immortal cell lines and cell lines from operative specimens (Table 1, Patients 4, 5, 8, 9, and 11). The immortal cell lines IOMM-Lee (A) and CH-157 MN (B) showed a greater percentage of cells in synthesis (S) phase when compared with the five benign cell lines analyzed (C–G). Benign meningiomas exhibited variability in the percent of cells in gap 1 (G1), synthesis (S), and gap 2 (G2). Error bars represent ±S.D.

UU IR Author Manuscript

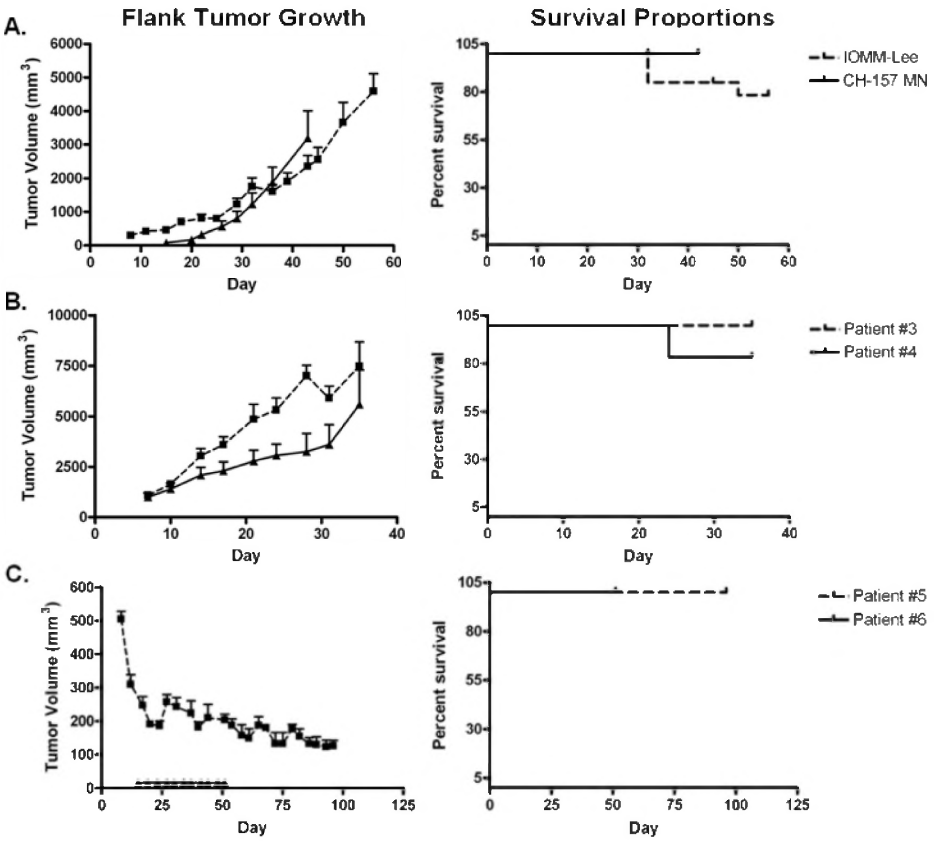

Figure 4: Line graphs depicting the growth of meningioma subcutaneous flank tumors, as well as corresponding mouse survival proportions. A. The immortal cell lines induced flank tumors in 95% (19/20) and 100% (10/10) of animals for the IOMM-Lee and CH-157 MN cell lines, respectively. Four of 20 (20%) animals died in the IOMM-Lee group, whereas no animals died in the CH-157 MN group. Animals were sacrificed after 43 days at varying times because of tumor size, per animal protocol. Error bars represent ±S.D. . B. Two complex karyotype cell lines (Patients 3 and 4) showed 100% (5/5) tumor induction. One (20%) of five animals with subcutaneous tumors induced from patient 4 died. All animals were sacrificed at 36 days because of tumor size, per animal protocol. Error bars represent ±S.D. C. Two simple karyotype cell lines incited tumors that did not grow (Patients 5 and 6). No animals died. Error bars represent ±S.D.

UU IR Author Manuscript

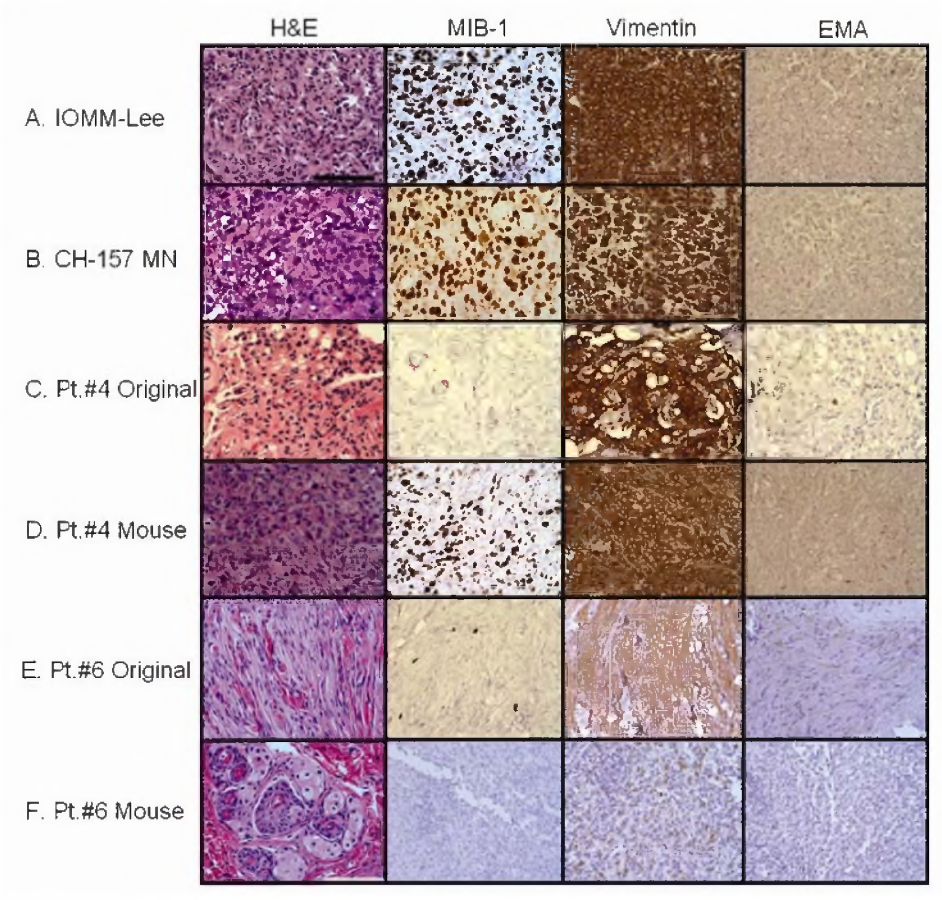

Figure 5: Representative histology and immunohistochemical staining slides of meningioma operative specimens and subcutaneous mouse flank tumors (40x objective, bar = 100 μm). A–B. Mouse flank tumors induced by the immortal cell lines IOMM-Lee (A) and CH 157-MN (B). C–F. Meningoma operative specimens and their corresponding subcutaneous mouse flank tumor. Representative tumors induced from a complex karyotype (C–D, Patient 4) and a simple karyotype (E–F, Patient 6) are shown. A–B. Both the IOMM-Lee (A) and CH-157 MN (B) flank tumors exhibited features of WHO III meningiomas of nuclear polymorphism, numerous mitosis, and high proliferative rates (MIB-1). CH-157 MN tumors resembled the WHO grade III rhabdoid meningioma subtype (e.g., large cells with eccentric nuclei and abundant cytoplasm).

UU IR Author Manuscript

Strong vimentin and weak EMA immunoreactivity was noted in both. C. The operative specimen from patient 4 showed H&E characteristics of a transitional meningoma (e.g., lobular pattern with occasional whorl-like structure), with sparse MIB-1 staining. D. The mouse flank tumor induced from patient 4 exhibited H&E similarities with the original operative specimen. However, in comparison with the original specimen, MIB-1 immunohistochemistry showed a much higher proliferative rate. Strong vimentin and weak EMA immunoreactivity was noted in both the operative and flank tumor specimens. E. The operative specimen from patient 6 showed H&E characteristics of a fibrous meningioma (e.g., parallel spindle cells with wide fascicles), with a few cells staining positive for MIB-1. F. Interestingly, the mouse tumor from patient 6 exhibited whorls, consistent with a transitional meningoma, unlike the original operative specimen. No cells stained positive for MIB-1. Moderate and weak vimentin immunostaining was noted in the operative and flank tumor specimen. Weak and no EMA immunoreactivity was observed in the operative and flank specimens, respectively.

UU IR Author Manuscript

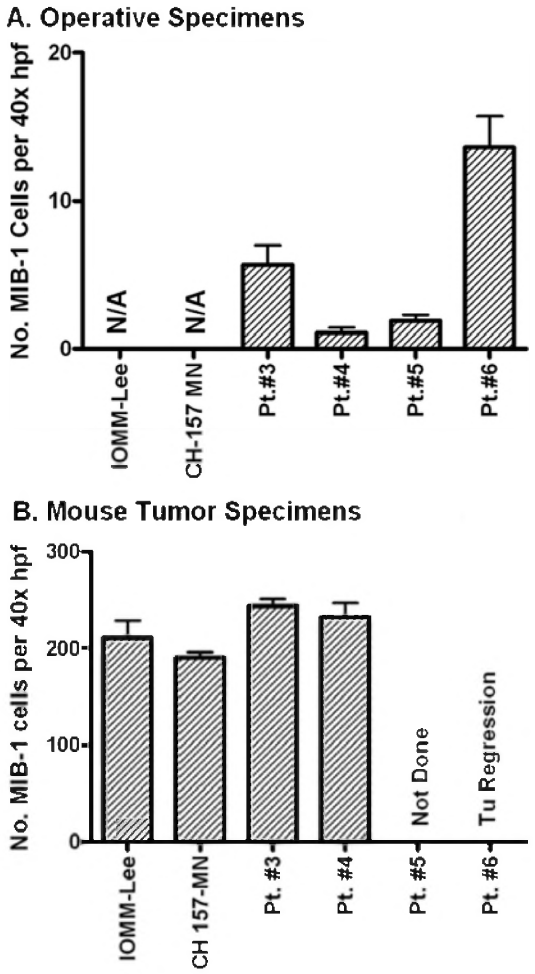

Figure 6: A–B. Bar graphs depicting the mean number of cells staining positive for MIB-1 in 40x high-powered fields (hpf) in the meningioma operative specimens (A) and mouse flank tumors (B). Error bars represent standard deviation (±S.D). A. The original operative specimens for the immortal cell lines were unavailable for analysis. The two operative specimens that induced mouse flank tumors showed MIB-1 counts of 5.7 ± 4.1 and 1.1 ± 1.1 for patients 3 and 4, respectively. The two operative specimens that showed tumor regression showed MIB-1 counts of 1.9 ± 1.3 and 13.6 ± 6.8, for patients 5 and 6, respectively. B. Cell lines inciting mouse tumors showed MIB-1 counts of ~200

UU IR Author Manuscript

per hpf (211.0 ± 75.7, 190.6 ± 23.8, 243.9 ± 30, 232.7 ± 60 for IOMM-Lee, CH-157 MN, and patients 3 and 5, respectively).

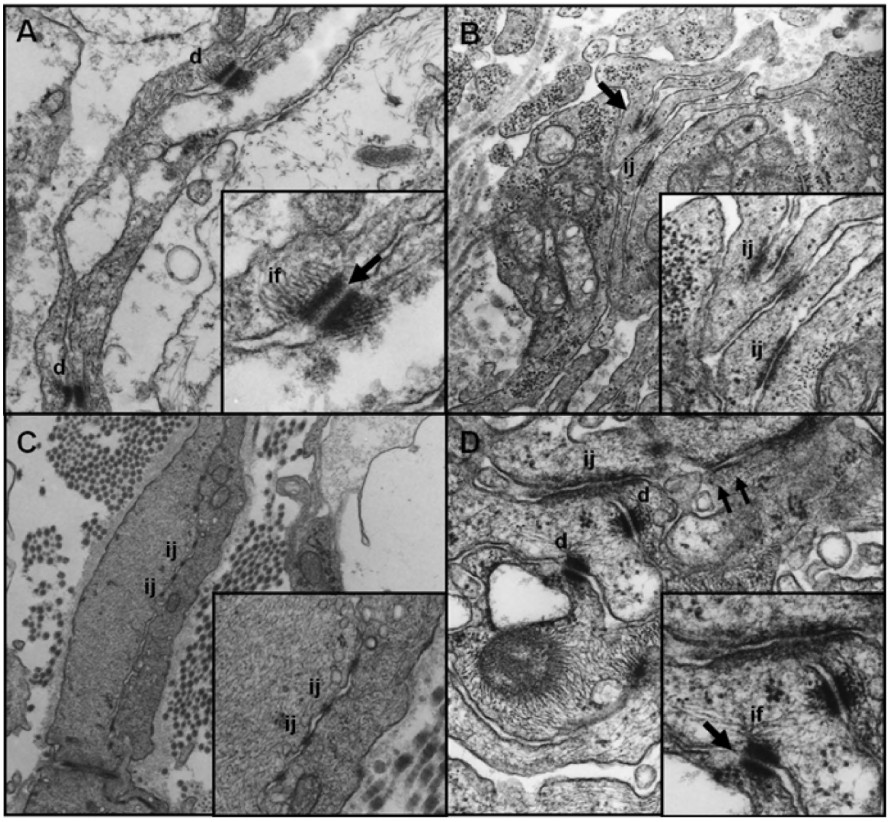

Figure 7: Transmission electron microscopy (TEM) pictures of a meningoma operative specimen (A) and meningioma mouse flank tumors (B–D). Three intercellular junction types have been described previously in meningiomas: Desmosomes (d), intercellular junctions (ij), and pentilaminar structures (double arrows). A. Patient 6, original operative specimen, exhibiting the key features of a desmosome: opposing disc-shaped plaques located on the cytoplasmic membrane, with inserting intermediate filaments (if), and an amorphous material present within the intercellular space (arrow). Original magnification is 33,782x and 86,004x (inset). B–C. IOMM-Lee (B) and CH-157 MN (C)

UU IR Author Manuscript

mouse flank tumors exhibited intercellular junctional (ij) complexes, which lack inserting intermediate filaments. IOMM-Lee original magnification 25,422x and 52,020x (inset). CH-157 MN original magnification 8,286x and 33,782x (inset). D. Patient 5, mouse flank tumor, exhibiting all three types of meningioma junctions. Original magnification 48,600x and 68,040x (inset).

UU IR Author Manuscript

Table 1: Characteristics of the meningiomas used in this comparison study

Patient no./Sex/Age	**Tumor Grade* / Subtype**	**Location**	**Model Number**	**Chromosomal Abnormalities**
1. IOMM-Lee. M / 61 (18)	WHO III	Intraosseous	48 (44 – 49)	X, -Y, -1, *add (2)(p11.2), add (5)(p13),* add (6)(p13), i(7)(p10)x2, add(9)(q21), **add(12)(q21)**, ***-17***, *add(14)(q13)*, add(19), *add(20)*, and +2-4 mar[p20].
2. CH-157 MN. F / 55 (36, 37)	Unknown	Unknown	73 – 82 <3n>	X, add (X)(p11.2), -X, add(1)(q21), add(1)(p13), *+2*, +3, *+5*, -1, i(8)(q10)x2, +8, add(11)(p11.2), +11, **+12**, *add(14)(p11.2)*, -15, i(15)(q10), -16, +16, ***-17***, -18, *+20*, -22, +4-9mar [cp10]
3. M / 71	WHO I / Meningothelial	Tentorial	47 (46 – 48)	**X, add(1)(p34), add(4)(p12), +del(5)(q31), add(6)(q27), +add(9)(p21), add(12)(q21)** [cp20]
4. M / 55	WHO I / Transitional	Convexity	47 (47 – 48)	**X, add(1)(p34), add(4)(p12), +del(5)(q31), add(6)(q27), +add(9)(p21), add(12)(q21)**, add(12)(q23)[cp20]
5. F / 71	WHO I / Transitional	Sphenoid Wing	48 (47 – 51)	XX, None
6. F / 41	WHO I / Fibrous	Parasagittal	46	XX, -22
7. F / 63	WHO I / Transitional	Cerebellopontine Angle	46	XX, None
8. F / 38	WHO I /	Olfactory Groove	45	**X, add(4)(p12)**, +5,**del(5q)(q22q31)**,

	Psammomatous			**add(6)(q23)**, +7, +9, **add(9)(q22)**, **add(12)(q13)** [cp10]
9. F / 49	WHO I / Transitional	Posterior Fossa		
10. F / 38 (NYG)	WHO I / Transitional	Paraclinoid		
11. F / 47	WHO I / Transitional	Cerebellopontine Angle		

(+) Entire chromosome addition, (-) entire chromosome deletion, (add) partial chromosome addition, (del) partial chromosome deletion.

Giemsa-band karyotyping was obtained on 8 meningiomas grown *in vitro*. Meningiomas studied exhibited a normal karyotype, a single chromosomal abnormality, or multiple chromosomal abnormalities. Text in boldface type indicates similar abnormalities between karyotyped meningiomas used in this study. Underlined text indicates meningioma chromosomal abnormalities reported in the literature. Italicized text indicates similarities between the immortal cell lines.

*Meningiomas were graded according to World Health Organization guidelines (21).

UU IR Author Manuscript

Table 2: Immunoreactivity of meningioma operative specimens and tumors grown in the mouse flanks.

	IOMM-Lee	CH-157 MN	Pt. 3	Pt. 4	Pt. 5	Pt. 6	Pt. 7	Pt. 8
Operative								
GFAP	N/A	N/A	-	-	-	-	N.D.	N.D.
Vimentin	N/A	N/A	+++	+++	+++	++	+++	+++
EMA	N/A	N/A	+	+	+	+	-	+
MIB-1	N/A	N/A	5.7±4.1	1.1±1.1	1.9±1.3	13.6±6.8	10.2±6.2	18.7±4.8
Mouse								
GFAP	-	-	-	-	N.D.	-	N/A	N/A
Vimentin	+	+	+	+	N.D.	+	N/A	N/A
EMA	+	+	+	+	N.D.	-	N/A	N/A
MIB-1	211.0±75.7	190.6±23.8	243.9±30	232.7±60	N.D.	0±0	N/A	N/A

(N/A) Not applicable, (N.D.) not done, (+++) strong, (++) moderate, (+) weak, (-) no immunohistochemical staining.

MIB-1 counts (mean ± SD).

UU IR Author Manuscript